



Chitosan-coated different particles in spouted bed and their use in dye continuous adsorption system

Claudio P. Pinheiro¹ · Tatiana G. Mello¹ · Mery L. G. Vieira¹ · Luiz A. A. Pinto¹

Received: 25 July 2018 / Accepted: 18 March 2019 / Published online: 30 March 2019
© Springer-Verlag GmbH Germany, part of Springer Nature 2019

Abstract

In this work, three polymer suspensions were used for coating glass beads (GB), porcelain beads (PB), and polyethylene pellets (PP) in spouted bed. Subsequently, the continuous adsorption assays of the food dye Brilliant Blue FCF in a fixed bed column were performed, which was packed with the covered particles. Also, the static adsorption assays were carried out. The adsorption equilibrium isotherms were fitted by Freundlich, Langmuir, and Temkin models, being that the Temkin model was the most suitable to represent the equilibrium data. The particle coating in the spouted bed showed promising results due to the high efficiency of the process. The PB, GB, and PP obtained coating efficiency values in the range to 92–96% when using the suspension of chitosan and hydroxyethyl cellulose. However, only the polyethylene particles coated with the chitosan suspension maintained its coating efficiency (95%). The maximum adsorption capacities at equilibrium of the coated particles of PP and GB were achieved with the chitosan suspension, being the values of around 800 mg g⁻¹. Thus, the chitosan-coated polyethylene particles showed to be a promising adsorbent for fixed bed column.

Keywords Dye adsorption · Fixed bed · Glass beads · Spouted bed · Polyethylene pellets · Porcelain beads

Introduction

Particle coating and drying are similar techniques in spouted beds, differing only by the interactions between the spray suspension and the particles. If the interaction is strong, the coating occurs and, on the contrary, drying takes place. The drying of liquids and pastes in spouted bed uses inert materials such as polyethylene, mainly for food compounds, because they do not contaminate the suspension (Larrosa et al. 2018). Rocha et al. (2009) demonstrated that the polyethylene

does not interact with the spray suspension at low temperature; however, the authors did not take into account the dielectric properties of polyethylene, which can create characteristics that favor the coating and not the suspension drying. The spouted bed can reach these characteristics and can produce conditions that allow the generation of an external electrostatic field, which interferes with the properties, piezoelectricity, and pyroelectricity of polyethylene. In addition, it is recognized that the spouted bed is one of the most versatile for gas–solid contact because of the efficient mixing provided (Prachayawarakorn et al. 2006; Niamnuay et al. 2011). Spouted beds are versatile and can be used in many applications, among them the skimmed milk drying over inert particles (Perazzini et al. 2017). Marshall (2017) showed that the spouted bed was suitable for the tristructural isotropic (nuclear fuel) that consisted of four layers, and each layer had a determined function. The thermal catalytic exploitation of vineyard pruning waste was made by José et al. (2018) in a conical spouted bed. Traditionally, conical spouted beds are used for Geldart D type particles. Pablos et al. (2017) found that using a modified conical spouted allowed operation with Geldart A, B, and D particles, with a small fraction of C particles. Niksiar and Nasernejad (2018) demonstrated that one-dimensional mathematical model can predict the behavior

Responsible editor: Angeles Blanco

✉ Luiz A. A. Pinto
dqmpinto@furg.br

Claudio P. Pinheiro
claudiopinheiro11@hotmail.com

Tatiana G. Mello
tati.guimello@hotmail.com

Mery L. G. Vieira
meryluiza@yahoo.com.br

¹ Industrial Technology Laboratory, School of Chemistry and Food, Federal University of Rio Grande—FURG, Rio Grande, RS, Brazil

of a spouted bed reactor during the gasification of char obtained from pyrolysis of pistachio shells leading to the production of activated carbons. This equipment ensures to the process high rates of heat and mass transfer and low pressure drops, being an excellent substitute for other coating techniques, such as dip coating and spin coating, which consist only in the application of large amounts of coating material on the inert particle surfaces (Wan et al. 2010; Soares et al. 2013, 2016).

Chitosan has many desirable characteristics, such as biocompatibility and biodegradability, renewability, and non-toxicity, but it has low selectivity, small surface area, low porosity, and has a tendency to form agglomerates or hydrogels, which limit its applications in adsorption. However, the ability of chitosan to acquire a cationic characteristic in an acid medium makes it a good adsorbent for dyes with an anionic characteristic (Dammak and Sobral 2018). This characteristic allows chitosan to interact with silicate minerals (Futalan et al. 2011), materials that have a negative charge on the surface or have some active site to interact as the amino groups of chitosan.

The batch adsorption method presents practical problems when applied on a large scale, and among them that can be featured are the difficulty of adsorbent separation from the aqueous solution, the adsorbent decantation, and longer times to reach equilibrium. Thus, the fixed bed column adsorption is receiving increasing attention since it presents an easy industrial scale-up, sorbent regeneration, and treatment of high wastewater volumes. However, the application of chitosan as an adsorbent in the form of flakes or powder presents limitations to the system, such as the hydrodynamic pressure drop and the column obstruction (Tan et al. 2009). Thus, the immobilization of chitosan on inert support is an alternative. This study aimed to use the coating process in a spouted bed to obtain particles coated with different polymer suspensions and to apply them as food dye adsorbent. The effects of particle type (glass, porcelain, and polyethylene) and of the chemical composition of coating suspension (chitosan and hydroxyethylcellulose) on the process efficiency were evaluated. In each type of particle coating, adsorption assay of the food dye Brilliant Blue FCF in fixed bed column was performed. The maximum capacity of the column was evaluated through the breakthrough curves.

Materials and methods

Materials

Shrimp waste (*Penaeus brasiliensis*) were acquired from local markets (Rio Grande, Brazil). Hydroxyethyl cellulose (Ashland), polyethylene glycol (PEG) 1500 grade (Synth),

and magnesium stearate (Sigma-Aldrich) were purchased from Company RF Química Ltda (Brazil). Porcelain beads (PB) were purchased from Porcelanas Rex S.A. (Brazil) and glass beads (GB) from Nacional Esferas Ltda. (Brazil). Polyethylene pellets (PP) were donated by the Drying Laboratory/School of Chemistry and Food, Federal University of Rio Grande (Brazil). Brilliant Blue FCF food dye was acquired from Duas Rodas Industrial Ltda (Brazil).

Chitosan production

Chitin was obtained from shrimp waste (*Penaeus brasiliensis*) by sequential chemical treatments of demineralization, deproteinization, and deodorization. Chitosan was obtained from chitin deacetylation reaction using sodium hydroxide solution 42.1% (solution/chitin ratio of 60:1, m m^{-1}), at 130 °C for 1.5 h of process, under constant agitation (50 rpm). The chitosan was purified and obtained in paste form, according to the procedures developed in our previous works (Weska et al. 2007; Moura et al. 2011; Moura et al. 2015), which was used to prepare the coating suspensions.

Suspension preparation

The suspensions used in the coating were composed of two polymer bases (chitosan and hydroxyethylcellulose), a plasticizer (polyethylene glycol) and a surfactant (magnesium stearate). The three different suspensions were prepared, and our compositions are shown in Table 1. The suspension preparation was carried out by dissolving each component separately in 3.0% (v/v) acetic acid solution under stirring at 500 rpm using a magnetic stirrer (Mars, MAG-01H, Brazil), at room temperature for 20 min. The reason to use acetic acid solution is because chitosan is insoluble in water). Afterward, the mixture of the components resulted in 1 L of suspension. The suspensions were stored in a refrigerated environment (4 ± 1 °C) until use.

Table 1 Chemical composition of the coating suspensions

Components	Suspensions		
	(A)	(B)	(C)
Hydroxyethylcellulose (g)	3.50	3.50	–
Chitosan (g)	–	5.00	5.00
Polyethylene glycol (g)	0.75	0.75	0.75
Magnesium stearate (g)	1.00	1.00	1.00
Concentration of solids (%) ^a	0.525	1.025	0.675

^a For 1 L of suspension

Material characterizations

Chitosan was characterized by the deacetylation degree through potentiometric linear titration and the molecular weight by the viscosimetric method using Mark–Houwink–Sakurada equation ($K = 1.8 \times 10^{-3} \text{ mL g}^{-1}$ and $\alpha = 0.93$) (Weska et al. 2007).

Coating suspensions were characterized in relation to the kinematic viscosity by a Cannon–Fenske capillary viscometer. The dynamic viscosity ($\text{kg m}^{-1} \text{ s}^{-1}$) was calculated by Eq. (1).

$$\mu = \nu \rho_{\text{susp}} \quad (1)$$

where ν is the kinematic viscosity ($\text{m}^2 \text{ s}$) and ρ_{susp} is the suspension density (kg m^{-3}).

The particles of glass, porcelain, and polyethylene were physically characterized by the mean diameter (D_m) and sphericity (ϕ) according to Rocha et al. (2009), being that 20 measurements were taken for each material to ensure a significant average. The bulk density (ρ) was obtained as the ratio of a mass known of particles and the volume occupied by them in a calibrated recipient. To each particle, which was inserted to the cell, was measured the D_c/D_i ratio, where D_c is the cell top diameter of each particle filling and D_i is the air inlet diameter.

Scanning electron microscopy (SEM) was used to characterize the particle surfaces, before and after coating, using an electron microscope (Jeol, JSM 6060, Japan) (Li et al. 2010).

The X-ray diffraction (XRD) (D8 Advance Bruker, USA) patterns of chitosan films (B) and (C) were obtained using a voltage of 40 kV and intensity of 40 mA. A copper tube was used with a wavelength (λ) of 15,418 Å (Saygili and Güzel 2016).

The functional groups of chitosan films (B) and (C) were identified by Fourier-transform infrared spectroscopy (FT-IR) (Prestige, 21210045, Japan) (Marques et al. 2018).

Coating in spouted bed

The particles used for the coating in spouted bed were glass beads, porcelain beads, and polyethylene pellets. Before coating, the particle surfaces were cleaned with an acid solution according to Vieira et al. (2014). The particle coating was carried out in a spouted bed with conical geometry, which was developed in our previous work (Larrosa et al. 2015). The equipment schema is presented in Fig. 1. The base and top of the equipment were composed by glass cones with enclosed angles of 60° (height 0.150 m, input and output diameters 0.029 m). In the middle part, there was a cylinder (height 0.150 m and diameter 0.175 m) where the double fluid spray nozzle (1/4J-SS + SUE18-SS; Spraying Systems Co., Brazil) was installed. The air was supplied by a radial blower (Ibram, model CR0850, Brazil) with 6 kW, heated by three electric resistances (2.4 kW). The air flow measurements were

taken using an orifice plate meter, and the heat control of the inlet air stream was carried out by a temperature controller (Contemp, IDO2B, Brazil).

Preliminary tests defined the operating conditions in order to guarantee stability in the bed. The minimum spouting velocity values for the studied particles were obtained by plotting the pressure drop as a function of air flow. The coating assays were conducted according to the following experimental conditions: air circulation rate 100% higher than the minimum spouted velocity, inlet air temperature of 80°C (353 K), and atomization pressure of 200 kPa abs. The suspensions were pumped at a flow rate of 5 mL min^{-1} using a peristaltic pump (MasterFlex, 07553-75, Canada), and they were atomized on the particles through a nozzle located 0.10 m above each particle bed. The particle load was 500 g and the processing time was 100 min. The coating assays were performed in triplicate.

After the coating process, curing method for chitosan fixation was used according to Vieira et al. (2014) with modifications. Curing physicochemical method consisted in drying with air circulation at 50°C for 12 h (physical), followed by immersion of the particles in a NaOH solution (1 mol L^{-1}) for 4 h (chemical), washing the particles with distilled water until neutral pH, and again drying. In this work, only the second step of the method was carried out (chemical) since the conditions of the spouted bed operation (air temperature of 80°C) provided an efficient rate of heat and mass transfer, thus, the solvent of the suspension was evaporated inside the bed.

Coating process efficiency

The coating efficiency evaluation was by Eq. (2), and the particles' relative growth was calculated by Eq. (3) (Donida and Rocha 2002; Vieira and Rocha 2004).

$$\eta = \frac{M_f - M_i}{W_{\text{susp}} C_{\text{sol}} t} \quad (2)$$

$$\delta = \frac{M_f - M_i}{M_i} \quad (3)$$

where M_f is the mass of coated particles (kg), M_i is the mass of the original particles (kg), W_{susp} is the volumetric flow rate of the suspension ($\text{m}^3 \text{ s}^{-1}$), C_{sol} is the solid concentration (kg m^{-3}), and t is the process time (s).

The solids adhered to the particles were quantified by peeling tests of the formed film. A sample obtained from a simple random sampling was placed in a beaker with a solution of acetic acid 3% (v/v), stirring at 900 rpm on a magnetic stirrer (Mars, MAG-01H, Brazil) for 30 min. The filtration was carried out for the separation, followed by washing the particles with distilled water and drying in an oven at $40 \pm 1^\circ \text{C}$ with air circulation until constant mass. Through Eq. (4), the adhered

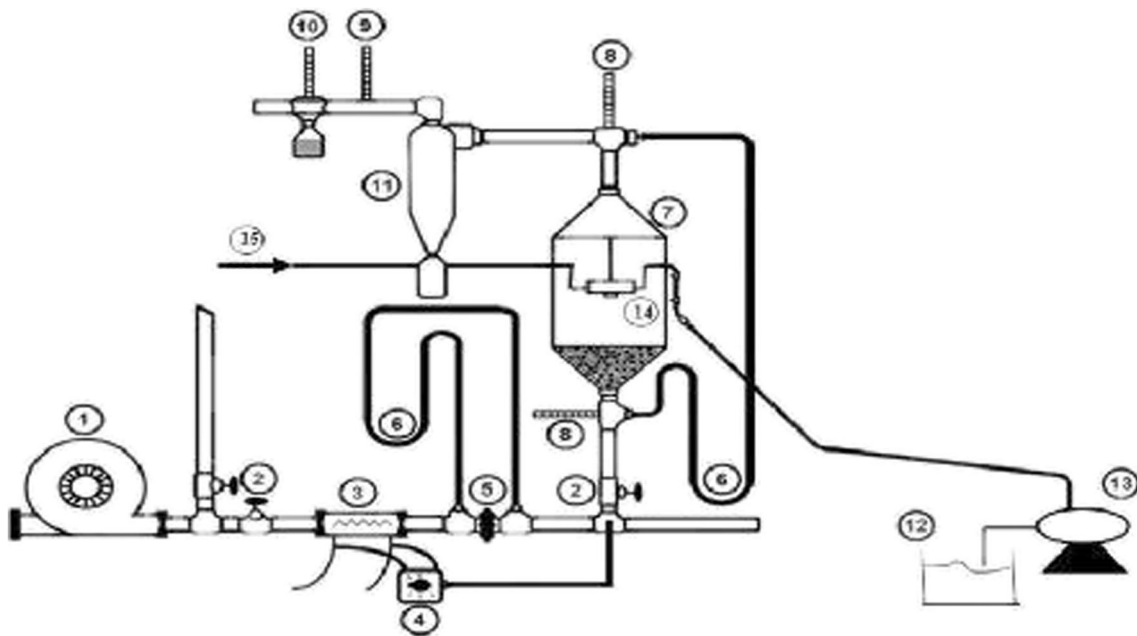


Fig. 1 Schema of the spouted bed equipment: (1) radial blower, (2) valves, (3) electric resistances, (4) temperature control, (5) orifice plate meter, (6) glass manometer, (7) spouted cell, (8, 9) dry bulb

thermocouples, (10) wet bulb thermocouple, (11) collector cyclone, (12) suspension tank, (13) pump, (14) spray nozzle, (15) compressed air line

mass of solids was determined. The peeling tests were carried out in triplicate.

$$M_{ader} = M_f - M_i \quad (4)$$

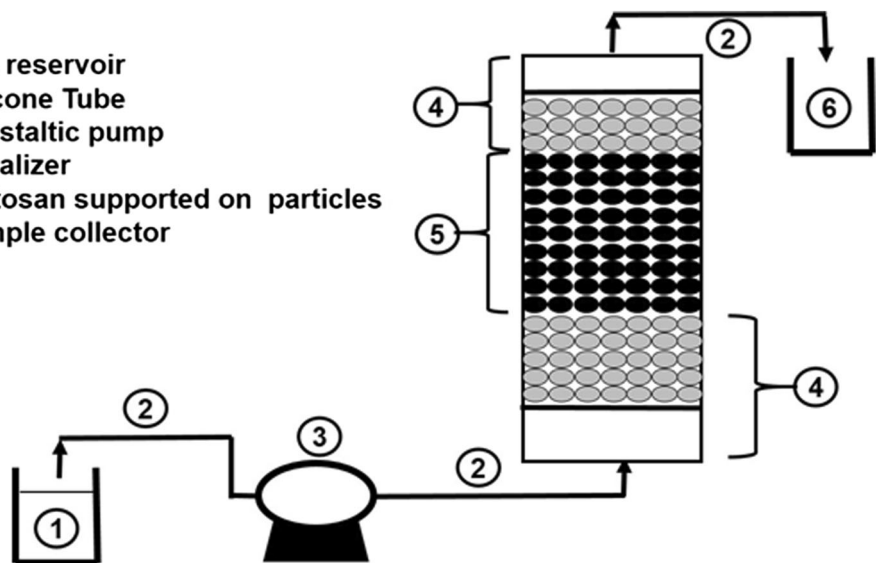
Application of the coated particles in adsorption on the fixed bed column and static adsorption experiments

The adsorption assays were carried out in an acrylic cylindrical column (internal diameter 3.4 cm and height 30.0 cm),

which was packed with the coated particles and coupled to a peristaltic pump (MasterFlex, 07553-75, Canada). The schema of the experimental unit of continuous adsorption is shown in Fig. 2. The dye solutions (100 mg L^{-1} and 298 K) flowed upward through the column at a flow rate of 5 mL min^{-1} , and the pH values were adjusted with a citric acid/disodium phosphate solution at pH 3 and 6. The column was packed with 10 cm of coated particles, and for the remainder of the column, uncoated inert particles were used. The samples were collected at regular intervals until the bed saturation, and the dye concentrations were determined by spectrophotometry (Quimis, Q108 DRM, Brazil), in wavelength of 630 nm.

Fig. 2 Schema of the continuous adsorption experimental unit: (1) dye reservoir, (2) silicone tube, (3) peristaltic pump, (4) equalizer (particles without coating), (5) particles coated with chitosan, (6) sample collector

- 1 – Dye reservoir
- 2 – Silicone Tube
- 3 – Peristaltic pump
- 4 – Equalizer
- 5 – Chitosan supported on particles
- 6 – Sample collector



The fixed bed saturation was considered when the outlet dye concentration was the same as the initial dye concentration. The assays were carried out in triplicate ($n = 3$), and blanks were carried out using uncoated particles.

The column data were analyzed by breakthrough curves (Chen et al. 2012; Acheampong et al. 2013). When the concentration of dye solution (C_t) reached about 5% of the initial concentration of dye solution (C_0), the breakthrough point is attained (t_b). The point where the concentration of dye solution reaches 95% is usually called the point of column exhaustion (t_e). The breakthrough curves usually are expressed by C_t/C_0 versus time. Equation (5) was used to calculate the effluent volume, V_{eff} (mL). The area under the breakthrough curve was used to determine the value of the total mass of adsorbed dye, m_{ad} (mg), Eq. (6). By Eq. (7), the equilibrium dye uptake or the maximum capacity of the column, q_{eq} (mg g^{-1}), was calculated; Eq. (8) was used to calculate the total amount of dye in the column (m_{total}) and the dye removal percentage R (%) was calculated from Eq. (9).

$$V_{eff} = Qt_{total} \tag{5}$$

where Q is the volumetric flow rate (mL min^{-1}) and t_{total} is the total flow time (min).

$$m_{ad} = \frac{Q}{1000} \int_{t=0}^{t=total} \left(1 - \frac{C_t}{C_0}\right) dt \tag{6}$$

where C_t is the adsorbed dye concentration (mg L^{-1}).

$$q_{eq} = \frac{m_{ad}}{m} \tag{7}$$

where m is the dry weight of adsorbent in the column (g).

$$m_{total} = \frac{QC_0 t_{total}}{1000} \tag{8}$$

$$R(\%) = \frac{m_{ad}}{m_{total}} \times 100 \tag{9}$$

The ratio t_b/t_e gives the fraction of the bed already used. Consequently, the length of the unusable bed, which corresponds to the mass transfer zone, can be determined according to Eq. (10).

$$ZTM = h \left(1 - \frac{t_b}{t_e}\right) \tag{10}$$

where h is the height of the column used (cm).

Static adsorption experiments were performed in batch mode. The amount of particles used was equivalent to 50 mg for the coating suspensions (B) and (C), respectively. The Brilliant Blue FCF concentrations were from 50 to 500 mg L^{-1} . The pH values were adjusted with a citric acid/disodium phosphate buffer solution at pH 3, with temperature of 298 K. After each experiment, the remaining dye

concentration in liquid phase was determined by spectrophotometry at 630 nm (Quimis, Q108 DRM, Brazil). Equilibrium adsorption capacity (q_e) was determined by Eq. (11), where C_0 is the initial dye concentration in liquid phase (mg L^{-1}), C_e is the equilibrium dye concentration in liquid phase (mg L^{-1}), m is the amount of adsorbent (g), and V is the volume of dye solution (L).

$$q_e = \frac{(C_0 - C_e)V}{m} \tag{11}$$

The adsorption equilibrium isotherms were fitted by Freundlich, Langmuir, and Temkin models (Piccin et al. 2011). These models are presented respectively in Eqs. (12), (13), and (14).

$$q_e = k_F C_e^{1/n} \tag{12}$$

$$q_e = \frac{q_m k_L C_e}{1 + (k_L C_e)} \tag{13}$$

$$q_e = \frac{RT}{b} \ln K_T + \frac{RT}{b} \ln C_e \tag{14}$$

The constants associated with the Freundlich isotherm model are sorption capacity (K_F) (mg g^{-1}) (L mg^{-1}) and sorption intensity ($1/n$). K_L is the Langmuir constant (L mol^{-1}) and q_m is the maximum monolayer adsorption capacity (mol g^{-1}). K_T is the Temkin constant (L mol^{-1}) corresponding to the maximum binding energy, b is related to the adsorption heat, R is the universal gas constant ($8314 \text{ J K}^{-1} \text{ mol}^{-1}$), and T is the temperature (K).

The nonlinear regression was performed to fit the column data. The parameters were determined through Quasi-Newton estimation method by use of the Statistic 7 software (Statsoft, USA). Tukey’s test was used to determine the significant differences ($p < 0.05$) between the data.

Results and discussion

Characterization of materials

Chitosan presented the degree of deacetylation of $85 \pm 1\%$ and the molecular weight of $146 \pm 5 \text{ kDa}$. In Table 2, the results for

Table 2 Dynamic viscosity and density of the different suspensions at 293 K

Suspension	Dynamic viscosity, μ ($\text{kg m}^{-1} \text{ s}^{-1}$)	Density, ρ_{susp} (kg m^{-3})
(A)	$0.04556 \pm 0.00012a$	$1004 \pm 2a$
(B)	$0.01352 \pm 0.00013b$	$1002 \pm 3a$
(C)	0.01199 ± 0.00013^c	1002 ± 3^a

Mean \pm standard deviation ($n = 3$). Different letters in same column indicate significant differences ($p < 0.05$)

the dynamic viscosity and the density of the suspensions are presented. This table shows that the suspensions presented significant differences ($p < 0.05$) because suspensions (B) and (C) had lower dynamic viscosity values than suspension (A); despite the density values of all suspensions, these did not present a difference ($p < 0.05$).

Figure 3 shows the XRD patterns of chitosan films with hydroxyethyl cellulose (B) and without hydroxyethyl cellulose (C). The two characteristic peaks of the chitosan are observed for (C), $(2\theta) = 15^\circ$ and 22° (Marques et al. 2018; Mohanasrinivasan et al. 2014; Prakash et al. 2012a). The first peak is assigned to *N*-acetyl-D-glucosamine sequences and the second peak to the sequences *N*-glucosamine in the polymer chain. The interactions between chitosan and hydroxyethyl cellulose (B) can have an effect on the second peak.

Figure 4 shows the infrared spectra for the obtained chitosan films (B) and (C). The main bands in their spectra are a broad band centered at $3250\text{--}3500\text{ cm}^{-1}$, corresponding to stretching vibrations of the O–H and N–H groups; the absorption peaks at 2875 cm^{-1} and 2920 cm^{-1} were attributed to the asymmetric and symmetric stretching vibrations of –CH groups; the band at 1082 cm^{-1} was assigned to the stretching of C–O–C in the glucose ring; there was an absorption band at 1651 cm^{-1} , corresponding to the amide of chitin; and the peaks around 901 and 1155 cm^{-1} were assigned to the saccharine structure (Schio et al. 2018; Prakash et al. 2016).

The particles were characterized in relation to the mean diameter (D_m), sphericity (ϕ), and density (ρ), and for each particle bed, D_c/D_i ratio was measured. Polyethylene pellets presented a different geometry of the glass and porcelain beads (Table 3 and Fig. 5). The geometry of the polyethylene pellets approached from two spherical caps; in addition, its density was lower than both beads, and the D_c/D_i ratio characterized this difference. The height that the PP occupied in the cone cell was the maximum possible, so the cell diameter

of the PP was the diameter of the upper part of the cone (0.175 m), leading to a smaller loss of suspension sprayed for the cone wall. In addition, a higher ratio approached the conventional spouted bed (CSB) and a lower ratio approached the jet spouted bed (JSB). The CSB is characterized by low velocity in the downward circulation of the particles in the annular zone, outside of the jet zone; however, the particles follow a fixed trajectory. When the cell depth is reduced, this leads to the JSB, and that involves an increase in mass transfer and heat transfer in the jet zone, presenting short residence times in the annular zone, but the bed becomes less stable and the particles do not have a fixed trajectory, thus a non-uniform coating can occur. The difference between CSB and JSB is in the D_c/D_i ratio, which for CSB is higher than 6, and in the bed porosity, which for CSB is less than 85%, and for JSB is higher. JSB presents a diluted annular region that contributes to the decrease in particle contact, which can reduce their agglomeration; however, its particle charge is lower than the CSB. Besides that, the JSB is also formed in the conical–cylindrical chamber, but solid particles are spouted by a high-velocity gas stream, which can lead to film detachment. The liquid material is usually atomized in the lower part of the JSB.

The beads of glass (GB) and porcelain (PB) presented similar characteristics ($p > 0.05$) in relation to the diameter, sphericity, and D_c/D_i ratio (Table 3). They differed only in their chemical composition, but both are composed of silica. However, the silica is scattered within three different phases (kaolin, feldspar, and quartz), each phase with a different percentage of silica. The glass is composed of approximately 75% silicon dioxide (SiO_2) (Tripathi et al. 2017). The presence of the silica is important for the interaction of the glass with chitosan, as demonstrated by Nawi et al. (2010) studying the

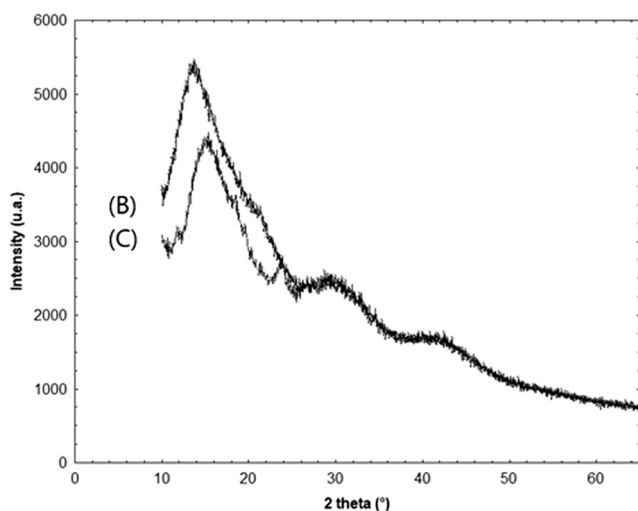


Fig. 3 XRD pattern of chitosan films (B) and (C)

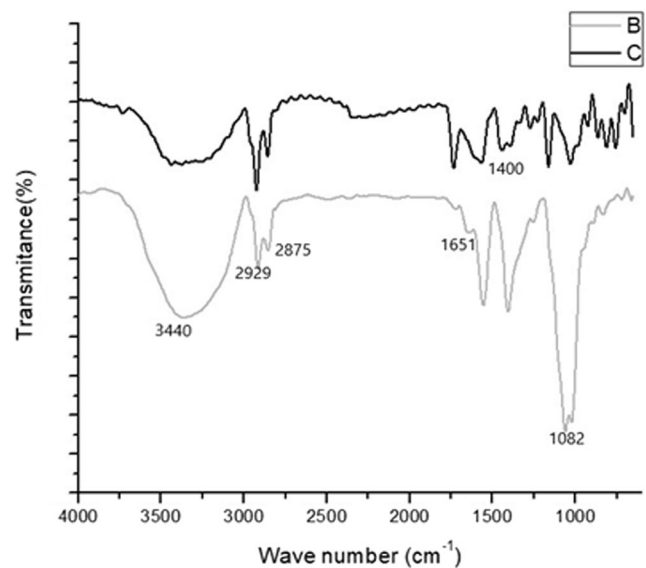


Fig. 4 FTIR spectra of chitosan films (B) and (C)

Table 3 Characterization of the different particles

Particle type	Particle mean diameter D_m (mm)	Sphericity ϕ	Density ρ (kg m ⁻³)	D_c/D_i ratio
GB	2.9 ± 0.1a	0.98 ± 0.02a	2418 ± 32a	4.1 ± 0.4b
PB	3.0 ± 0.1a	0.97 ± 0.02a	2468 ± 40a	4.4 ± 0.3b
PP	3.2 ± 0.2a	0.70 ± 0.03b	960 ± 10b	6.1 ± 0.4a

Mean ± standard deviation ($n = 3$). Different letters in column indicate significant differences ($p < 0.05$)

GB, glass beads; PB, porcelain beads; PP, polyethylene pellets

immobilization of chitosan on glass plates and Vieira et al. (2014) studying coating chitosan on glass beads. These authors verified that the use of an acid solution of chitosan can acquire a positive charge in an acid medium and interact with the SiO_4^{4-} tetrahedral units on the glass surface. Thus, the degree of deacetylation is an important characteristic of chitosan since it is proportional to the number of free amino groups, which in acid medium can be protonated (NH_3^+). In addition, the free amino groups are responsible for the main characteristics of chitosan (Dotto et al. 2016).

The formation of a negative electric layer on the polyethylene surface in contact with aqueous solutions can explain this interaction, and Beneš and Paulenová (1973) studied this phenomenon. The authors observed that the adsorption of Ba^{2+} ions occurred only in a pH region (where the polyethylene surface was negatively charged); the same occurred for the adsorption of other cations on polyethylene. In addition, Hashimoto et al. (1975) demonstrated that the minimum electric field required for the generation of an electric current by the polyethylene is 100 kV/cm for the temperature of 90 °C, being that a negative peak appeared in thermally stimulated current spectra for temperatures above 67 °C, and the peak increased with increasing polarization temperature. Thus, the characteristic cyclic motion in which the particles are subjected within the spouted bed generates countless collisions and frictions between the polyethylene particles together with the inlet temperature of the fluid at 80 °C, which may lead to the generation of a negative charge on the polyethylene pellets. This may thus interact with the amino groups that are protonated in an acid medium. The spouted bed can activate the

carboxyl groups that the synthesis of the polyethylene generated, creating active sites to interact with the chitosan. Pâslaru et al. (2013) performed a similar procedure for the formation of a covalent bonding between chitosan and the polyethylene surface in a two-step procedure, through corona treatment of the polyethylene surface and its chemical activation.

Scanning electron microscopy

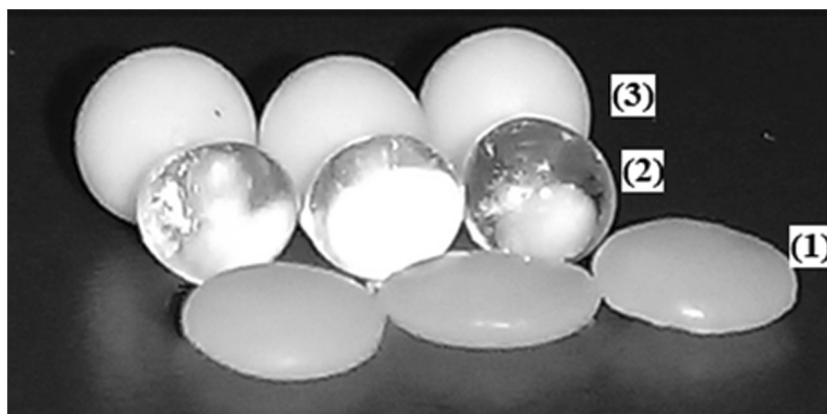
Suspension (C) generated a less smooth surface than the other two suspensions (Fig. 6). This can be a positive factor for adsorption because it increases the surface area. The smooth surface presented in suspensions (A) and (B) can be attributed to the presence of hydroxyethyl cellulose, as it is a gelling and thickening agent, and exhibits good water retention (Amirkhani et al. 2008).

Due to the evaporation of acetic acid during coating, chitosan tends to coagulate. Thus, its structure and mechanical properties can change because these are pH dependent. The increase of pH or of the polymer concentration leads to an increase of elastic modulus in chitosan systems due to the change of crosslinking patterns. Parallel crosslinking is dominant when the polymer concentration is low, while at higher polymer concentration both crosslinking in parallel and perpendicular play an important role (Xua and Matysiak 2017).

Process efficiency of coating in spouted bed

The drying and the coating in the spouted bed are two techniques that differ mainly by the interaction between

Fig. 5 Digital photograph of all the beads: (1) polyethylene pellets; (2) glass beads; (3) porcelain beads



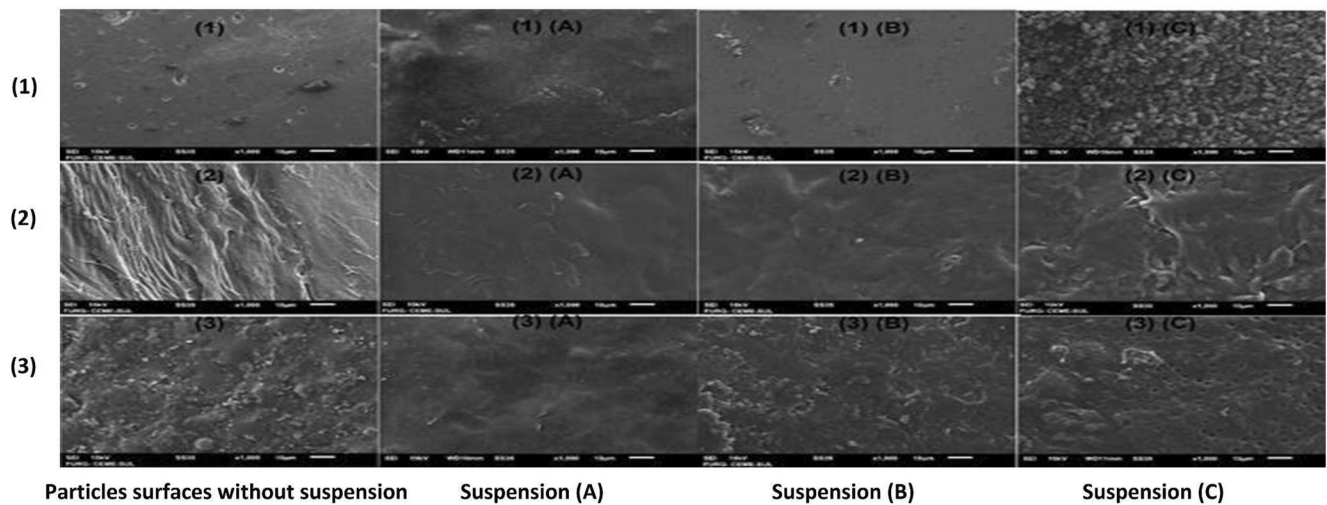


Fig. 6 Scanning electron microscopy (SEM): (1) glass beads; (2) polyethylene pellets; (3) porcelain beads

solid and liquid. If the interaction is strong enough, the coating occurs; on the contrary, the material drying occurs. This interaction can be quantified by the contact angle. Rocha et al. (2009) showed that contact angles lower than 70° result in the coating and above 76° result in drying, as high contact angles indicate worse wettability and, consequently, weak adhesion. In addition, the authors using a suspension similar to suspension (A) used in this work, and polystyrene, polypropylene, and low-density polyethylene as the inert particles, found that the coating did not adhere, the drying of suspension occurring only using an air temperature of 60 °C. The values presented in Table 4 show opposite results to those presented by the authors. This may be associated with the negative peak observed in the thermally stimulated current spectra for the polyethylene (Hashimoto et al. 1975). Thus, the coating observed in this work is associated with the use of a higher temperature (80 °C), which can stimulate a negative charge on the surface of the polyethylene. The suspensions were characterized in relation to the dynamic viscosity and its

influence was evaluated regarding coating efficiency. The suspensions with chitosan (B) and (C) presented a result superior for the coating efficiency and relative growth compared to suspension (A) (Table 4) because a lower drying of suspensions (B) and (C) occurred. This result may be associated with the dynamic viscosity value differences between the suspensions (Table 2). Chitosan suspensions exhibit lower dynamic viscosity values, so it is expected that a suspension with a lower viscosity will have a better wettability because when the droplets reach the particles, these can spread over a larger radius before being dried. The dynamic viscosity of suspension (A) was higher than suspensions (B) and (C), and it can be attributed to the presence of the hydroxyethyl cellulose because it is partially soluble in acetic acid. Hydroxyethyl cellulose provides protective colloid action, and this can influence viscosity, such as water retention. Hydroxyethyl cellulose is manufactured in a variety of viscosity grades, and its viscosities can range from as low as 0.01 kg m⁻¹ s⁻¹ up to 100 kg m⁻¹ s⁻¹. Besides that, a similar behavior was observed

Table 4 Adhesion efficiency (η) and relative growth (δ) of the particles coated with the suspensions

	Particles	Suspension (A)	Suspension (B)	Suspension (C)
η (%)	GB	25 ± 02cC	93 ± 1bA	88 ± 2bB
	PB	50 ± 3bC	92 ± 1bA	70 ± 1cB
	PP	67 ± 2aB	96 ± 1aA	95 ± 1aA
δ (kg _{solid} kg ⁻¹ particle)	GB	0.0011 ± 0.0002cC	0.0095 ± 0.0001bA	0.0060 ± 0.0002aB
	PB	0.0023 ± 0.0003bC	0.0094 ± 0.0001bA	0.0048 ± 0.0003bB
	PP	0.0035 ± 0.0003aC	0.0098 ± 0.0001aA	0.0064 ± 0.0003aB
Mass adhered (mg _{solid} g ⁻¹ particle)	GB	0.66 ± 0.02cC	4.77 ± 0.02aA	2.99 ± 0.09bB
	PB	1.31 ± 0.01bC	4.71 ± 0.02bA	2.38 ± 0.08cB
	PP	1.76 ± 0.01aC	4.77 ± 0.03aA	3.21 ± 0.10aB

Mean ± standard deviation (n = 3). Different lowercase letters in same column indicate significant differences (p < 0.05). Different uppercase letters in same line indicate significant differences (p < 0.05)

GB, glass beads; PB, porcelain beads; PP, polyethylene pellets

by Rocha et al. (2009). Another relevant factor is the presence of chitosan that creates active sites, which can interact with the particles in a stronger way. In addition, the solid concentration in suspension (A) was lower than the other suspensions (Table 1), so the film formed on the particles was thinner, and the relative growth appears proportional to the suspension solid concentration. This behavior regarding the significant influence of solid concentration on particle growth is confirmed in other works in the literature (Souza et al. 2009; Rocha et al. 2009). Thinner films are longer exposed to the fluid, and due to the drying and the collisions between the particles, film detachment may occur. The type of particle used for bed coating had a significant influence on the process efficiency. In general, it can be seen in Table 4 that the highest values for coating efficiency were found when the polyethylene pellets were used for all suspensions under study. In addition, it can be noticed that suspension (B) stood out from the others, maintaining efficiency values above 92% for all the studied particles. In this way, it can be inferred that the presence of both polymers in the coating suspension contributed to the stability in the process efficiency values.

The coating efficiency for porcelain beads (PB) was twice that found for glass beads (GB) relative to suspension (A) (Table 4). Although both particles have similar physical and chemical characteristics, this difference may be associated with the rough surface of the porcelain, while the surface of the glass is smooth (according to SEM images in Fig. 6). The superior result found for the polyethylene pellets (PP) may be associated with a higher D_o/D_i ratio, as it results in lower loss of the suspension to the wall, in addition to a possible electric charge formed on the surface of the PP. The effect of particle type on efficiency was less pronounced when suspension (B) was used. The PP had an efficiency slightly higher than that found for the coating with GB and PB. The difference observed may be associated with the behavior of the particles within the bed. The PP occupied more space inside the bed and its operational conditions were closer to the conventional spouted bed (CSB), while for GB and PB, the conditions were closer to the jet spouted bed (JSB).

The particle type had a significant influence on the coating when suspension (C) was used. The values for the coating efficiency followed the order $PP > GB > PB$. These results may be associated with the presence of chitosan in the suspension, which interacts more strongly with the polyethylene particles, either by its electron-loaded surface or by its spherical cap geometry, favoring the coating. On the other hand, the particles of glass and porcelain present silica in their composition. According to Heise et al. (2018), the isoelectric point of silica in water is at pH 1.6. At a higher pH, the zeta potential is negative. They showed that the glass beads had a zeta potential of -41 mV in water and, in the presence of chitosan, the zeta potential was around $+50$ mV. However, as in glass there are more tetrahedral units in the surface layer, the interaction

between silica and chitosan present in the suspension was more effective in GB than in PB. Rocha et al. (2018) presented coating efficiencies ranging from 40% to 93% using a spouted bed. Jawad et al. (2017) performed the coating of glass plates with modified chitosan to remove the reactive Orange 16 dye; however, they found a lower percentage of immobilized chitosan (≈ 1.25 mg cm⁻²). Vieira et al. (2018) demonstrated that chitosan with degree of deacetylation 85% was better for the glass beads coating and in bed adsorption performance for azo dye, and the coating was performed by dip-coating technique, obtaining 2.63 mg_{chitosan} mg_{beads}⁻¹.

The superior results presented by the PP can be associated with the particle density because denser materials (GB and PB) provide more vigorous collisions, leading to film detachment.

In the present work, a plasticizer (polyethylene glycol) was used, which may have favored the coating since its function is to improve the flexibility of the polymers, penetrating in the middle of the polymer chains and, thus, increasing the free space between the chains (Zelkó et al. 2002). Besides that, Heinämäki et al. (1994) demonstrated that the water vapor permeability of the films decreased with an increased molecular weight of the polyethylene glycol when compared with unplasticized control films. According to Mota (2013), polyethylene glycol is hydrophilic and can leach from the films creating porosity. Studies of drug release showed that complete release was achieved due to the PEG leaching, which created porosity and facilitated drug diffusion. Thus, the grade 1500 of the polyethylene glycol may favor the adsorption.

Adsorption in fixed bed column

The adsorption assays of the Brilliant Blue FCF food dye in fixed bed were performed. This dye has their sulfonate groups dissociated and converted into anions in acid pH (Tutunaru et al. 2017). Thus, the interaction between chitosan and the adsorbate may occur more efficiently at acid pH (Piccin et al. 2009). Popuri et al. (2009) reported that the chitosan functional groups ($-\text{NH}_2$, $-\text{OH}$) remained intact after the PVC coating.

Several works have used chitosan-coated material as adsorbent, such as chitosan-coated attapulgite (Deng et al. 2012), chitosan-coated bentonite beads (Calagui et al. 2014), and fly ash coated by chitosan (Adamczuk and Kołodynska 2015). The methodology used in these adsorbent preparations presented a step of mixing and/or contacting the material to be coated with the chitosan, followed by a step of chitosan adhesion to the material. The adhesion step was performed by coagulation (chemical cure) or drying (physical cure). For the chitosan coagulation, an alkaline solution was used. The drying was carried out at temperatures ranging from 60 to 105 °C. Gama et al. (2018), using bead glass coated with chitosan for the removal of copper in a fixed bed, found that the highest removal rate occurred when the lower flow rates

were applied to the initial concentration of 100 mg L^{-1} . In a previous work using dip-coating technique (Vieira et al. 2014), it was observed that in the cure method for the glass beads covered with a chitosan solution, the physicochemical process positively influenced the adhesion of chitosan to the glass surface. Thus, adsorption assays were carried out to evaluate the cure method effect on the particles coated with suspension (A), with only the polymer hydroxyethylcellulose. The breakthrough curves are shown in Fig. 7. The release of the film occurred in the GB and PB that did not undergo the cure method, interfering with the concentration reading of the samples. However, there was no influence on the PP, where it was possible to adsorb with and without cure method. This indicated that the interaction between PP and suspension was different in relation to GB and PB. The values of the maximum capacity of the column, q_{eq} (mg g^{-1}), were 2.46 ± 0.26 for PB, 3.85 ± 0.32 for GB, and 2.59 ± 0.12 for PP, all with cure method. However, the q_{eq} value for PP without the cure method was $3.77 \pm 0.26 \text{ mg g}^{-1}$. Although the presence of hydroxyl groups (OH^-) of the hydroxyethylcellulose may have contributed to adsorption, the adsorption capacity was low in this polymer; in addition, the materials were not porous (SEM images in Fig. 6).

The breakthrough curves for dye adsorption onto the particles coated with suspensions (B) and (C) are shown in Figs. 8 and 9, respectively. It can be seen in Figs. 8 and 9 that the breakthrough curves obtained do not follow a characteristic profile “S” produced in ideal adsorption systems. The “S” shaped profile is associated with adsorbents with small molecular diameters and simple structures, which are not true for most dyes. However, the dye adsorption (at pH 3) showed high values of maximum column capacity (q_e), reaching 708 mg g^{-1} for GB coated with suspension (B) and

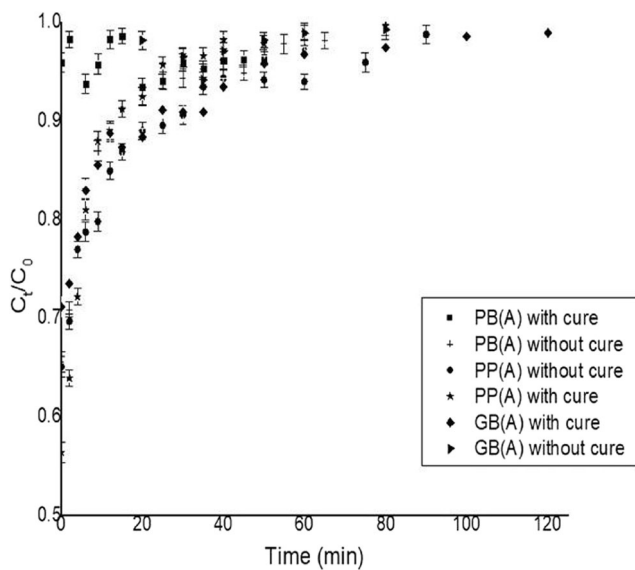


Fig. 7 Breakthrough curves for the adsorption of Brilliant Blue FCF, with and without cure method, for suspension (A), at pH 3

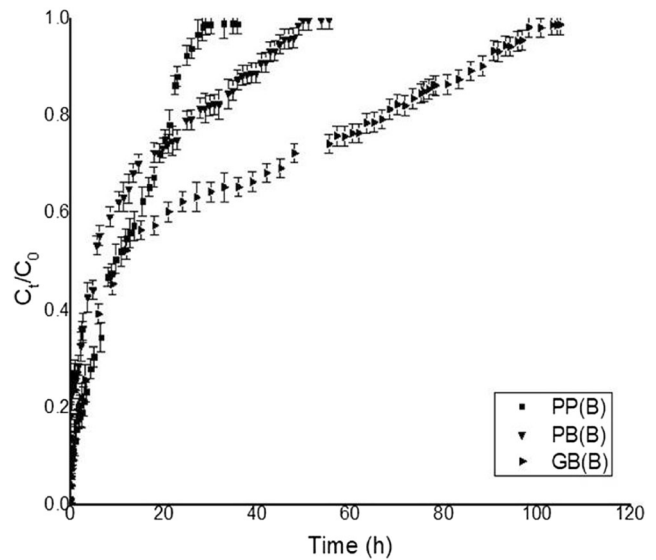


Fig. 8 Breakthrough curves for the adsorption of Brilliant Blue FCF for particles coated with suspension (B), at pH 3

815 mg g^{-1} for PP coated with suspension (C), as shown in Table 5. For the particles coated with suspension (B), the best adsorption capacity of the column was found for GB, followed by PP and PB. The polyethylene pellets (PP) presented a value of q_e slightly lower than that of the glass beads (GB); however, the time to saturation was much lower for PP (about 30 h) compared to more than 100 h for GB. Opting for the application of PP coated for adsorption results in great energy savings, in addition to the fact that polyethylene is a cheaper material than glass. For the particles coated with suspension (C), the best adsorption capacity of the column was found for PP, followed by GB and PB. This fact may be associated with the mass of adsorbent (chitosan) present in the particles since the mass of solids that adhered to the particles was 3.2 mg g^{-1}

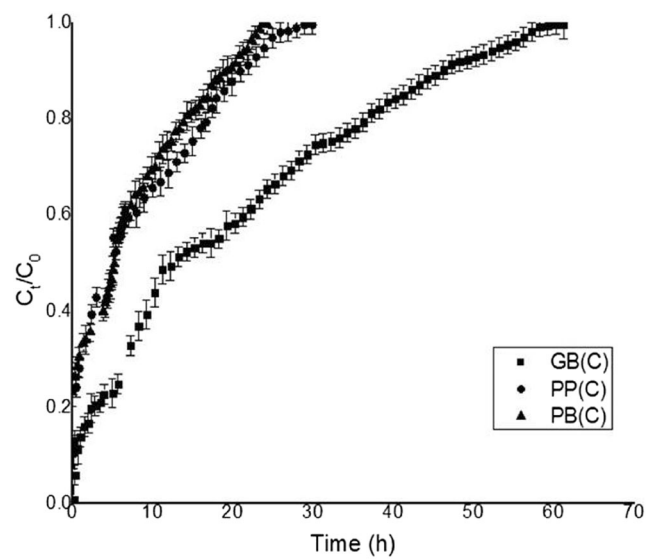


Fig. 9 Breakthrough curves for the adsorption of Brilliant Blue FCF for particles coated with the suspension (C), at pH 3

Table 5 Operation characteristics for the adsorption of Brilliant Blue FCF dye in the fixed bed column at pH 3

		t_{total} (h)	V_{eff} (L)	m_{ad} (mg)	q_{eq} (mg g ⁻¹)	m_{total} (g)	R (%)	ZTM (cm)
Suspension (B)	GB	103.3 ± 0.5a	30.98 ± 3.02a	914 ± 12a	708 ± 26a	1.290 ± 0.012a	29.5 ± 0.4b	9.96 ± 0.02
	PB	49.8 ± 0.7b	14.95 ± 2.49b	376 ± 4b	414 ± 17c	0.480 ± 0.012c	25.1 ± 0.5c	–
	PP	29.0 ± 0.3c	8.70 ± 1.70c	331 ± 3c	619 ± 21b	0.910 ± 0.010b	38.1 ± 0.5a	–
Suspension (C)	GB	61.3 ± 0.7a	18.38 ± 0.87 ^a	581 ± 12a	777 ± 12b	1.838 ± 0.012a	31.6 ± 0.6a	9.95 ± 0.56a
	PB	24.3 ± 0.6c	6.85 ± 0.72c	214 ± 8c	360 ± 11c	0.685 ± 0.013c	31.3 ± 0.5a	–
	PP	29.9 ± 0.3b	8.98 ± 0.82b	241 ± 9b	815 ± 9a	0.898 ± 0.008b	26.9 ± 0.5b	–

Mean ± standard deviation ($n = 3$). Different letters in the column for each suspension indicate significant differences ($p < 0.05$)

GB, glass beads; PB, porcelain beads; PP, polyethylene pellets

for PP, 3.0 mg g⁻¹ for GB, and 2.4 mg g⁻¹ for PB (Table 4). In addition, GB and PP had the best adsorption capacity when coated with suspension (C). This behavior can be attributed to the fact that the effective mass of adsorbent was higher in this suspension containing only chitosan, while in suspension (B), there was also the presence of hydroxyethylcellulose, which has a lower adsorption capacity.

To demonstrate the influence of pH, dye adsorption assays with the particles coated with suspension (B) at pH 6 were performed. The maximum column capacity values were 7.84 ± 1.34, 1.50 ± 0.08, and 0.72 ± 0.04 mg g⁻¹ for PP, PB, and GB, respectively. These results confirm the literature data about chitosan, and the increase in pH provides a reduction in the number of protonated amine groups. The soluble–insoluble transition of the chitosan occurs around a pH between 6 and 6.5 (Zargar et al. 2015; Cadaval et al. 2016; Withers 2017), and the dye presents a neutral form at this pH (German-Heins and Flury 2000), thus, there is no interaction between the two. Salih and Ghosh (2018) performed the Zn (II) adsorption in a bed fixed using diatomaceous earth covered with chitosan through the drop-wise method. The continuous adsorption studies showed a decrease of the

breakthrough and exhausted times with the increase of the solution flow rate. In addition, they demonstrated that the pH point of zero charge was at pH 5.8 and that the positive zeta potential at low pH was created by the protonation of amine groups in chitosan. To evaluate the difference between PP and GB, an adsorption assay was performed with the same mass adhered (suspension (B)) to the PP, equivalent to the 10 cm occupied by the GB. Thus, the height occupied by the PP was 24 cm. The maximum capacity of the column was 862 ± 28 mg g⁻¹, and this superior result is due to the longer time that the dye interacted with the chitosan.

The adsorption showed for lower of C_e values a strong affinity of the adsorbent with the dye (Figs. 10 and 11). However, the curves reached approximately a plateau at higher C_e values, indicating that the adsorbent surface was saturated with the dye. The equilibrium curves were fitted by Langmuir, Freundlich, and Temkin models. Table 6 shows the equilibrium parameters for the dye adsorption onto coated particles. The glass beads and polyethylene pellets showed a similar behavior; however, the porcelain beads presented a different behavior, and this can be observed by the values of R^2 . In general, the Temkin model was the most adequate to represent the equilibrium data due to the high values of the

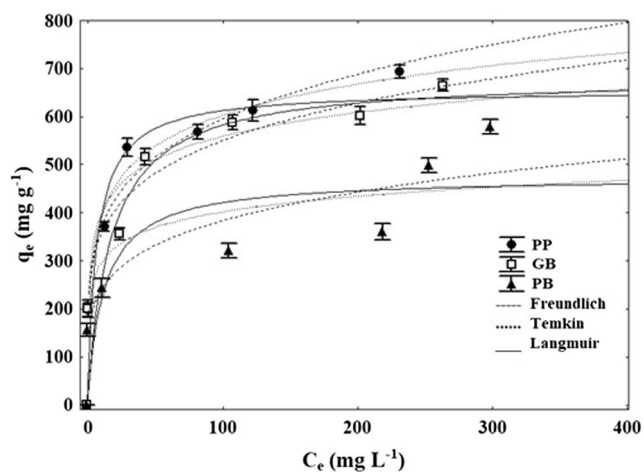


Fig. 10 Adsorption equilibrium isotherms and fitting Freundlich, Langmuir, and Temkin models for particles coated with the suspension B, at pH 3

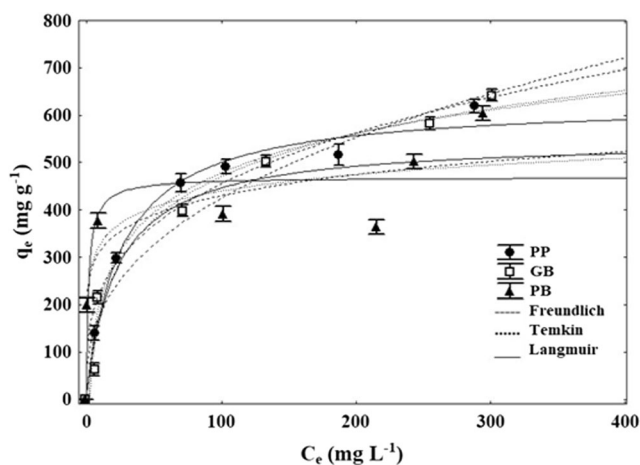


Fig. 11 Adsorption equilibrium isotherms and fitting Freundlich, Langmuir, and Temkin models for particles coated with the suspension (C), at pH 3

Table 6 Equilibrium parameters for the adsorption of Brilliant Blue FCF onto the particles coated with the suspensions (B) and (C)

Isotherm models	(B)			(C)		
	GB	PP	BP	GB	PP	PB
q_m (experimental)	665 ± 15	642 ± 18	619 ± 12	603 ± 15	693 ± 12	578 ± 16
Freundlich						
K_f (mg g ⁻¹)(L mg ⁻¹)	95.5	70.2	60.2	56.3	110.4	51.6
1/n	0.343	0.331	0.221	0.303	0.206	0.308
R^2	0.9740	0.9549	0.9729	0.8153	0.9763	0.8917
ARE (%)	12.54	20.47	19.12	7.67	6.32	11.65
Langmuir						
q_m (mg g ⁻¹)	565	559	538	498	620	488
K_L (L mg ⁻¹)	0.311	0.456	0.322	0.521	0.234	0.401
R^2	0.8699	0.9573	0.9883	0.7894	0.9455	0.7317
ARE (%)	8.49	11.23	14.45	22.12	12.24	9.51
Temkin						
K_T (L mol ⁻¹)	9.34 × 10 ⁴	1.29 × 10 ⁷	3.76 × 10 ⁴	4.23 × 10 ⁶	7.32 × 10 ⁵	4.34 × 10 ⁵
b × 10 ⁶	16.8	26.6	10.4	15.4	12.1	15.2
R^2	0.9560	0.9937	0.9926	0.8160	0.9868	0.8419
ARE (%)	11.63	8.42	9.33	12.77	11.54	12.28

Mean ± standard deviation (n = 3)

GB, glass beads; PB, porcelain beads; PP, polyethylene pellets

coefficient determination and the low values of the average relative error. The model assumes that heat of adsorption of all molecules in the layer would decrease linearly rather than logarithmic with coverage; however, the model does not offer information on maximum adsorption capacity. The values of q_m of the Langmuir model approximated the values obtained experimentally. In the Freundlich model, the smaller exponents mean that sorbents are bound with weaker and weaker free energies (Prakash et al. 2012b). The smallest exponent was found for polyethylene pellets, and the glass beads and porcelain beads showed similar values.

Conclusions

The particles of porcelain (PB), glass (GB), and polyethylene (PP) were coated in spouted bed with suspensions containing the polymers hydroxyethylcellulose (suspension (A)), hydroxyethylcellulose and chitosan (suspension (B)), and chitosan (suspension (C)). The spouted bed was composed by glass cones with enclosed angles of 60°, a height of 0.150 m, and inlet and outlet diameters of 0.029 m. In the middle part, there was a cylinder with a height of 0.150 m and a diameter of 0.175 m. Suspension (A) showed low values of efficiency. In contrast, suspension (B) presented the best results of process efficiency with values of 92%, 93%, and 96% for PB, GB, and PP, respectively. For suspension (C), the PP have maintained their efficiency around 95%. Through analysis of XRD and

FT-IR, films (B) and (C) were characterized and evidenced the presence of chitosan. For the static adsorption assays in general, the Temkin model was the most suitable to represent the equilibrium data. The values of q_m of the Langmuir model were close to the experimental values. The spouted bed technique proved to be feasible for the coating of different particle types, and the polyethylene pellets showed a high coating percentage. The best results for the food dye Brilliant Blue FCF adsorption in the fixed bed column with coated particles were obtained at pH 3, using glass beads (GB) and polyethylene pellets (PP) coated with chitosan suspension (C), reaching adsorption capacities of the column of 777 mg g⁻¹ and 815 mg g⁻¹, respectively. These results are promising since the polyethylene presents a lower cost, besides the possibility to extend its application in dye adsorption area.

Acknowledgments The CAPES (Coordination for the Improvement of Higher Education Personnel—Finance Code 001) and CNPq (National Council for Scientific and Technological Development) supported this work. Furthermore, the authors would like to thank CEME–SUL/FURG (Electron Microscopy Center of Southern/Federal University of Rio Grande) for the scanning electron microscopy images.

References

Acheampong MA, Pakshirajan K, Annachatre AP, Lens PN (2013) Removal of Cu(II) by biosorption onto coconut shell in fixed-bed column systems. *Ind Eng Chem* 19:841–848. <https://doi.org/10.1016/j.jiec.2012.10.029>

- Adamczuk A, Kolodynska D (2015) Equilibrium, thermodynamic and kinetic studies on removal of chromium, copper, zinc and arsenic from aqueous solutions onto fly ash coated by chitosan. *Chem Eng J* 274:200–212. <https://doi.org/10.1016/j.cej.2015.03.088>
- Amirkhani M, Volden S, Zhu K, Glomm WR, Nyström B (2008) Adsorption of cellulose derivatives on flat gold surfaces and on spherical gold particles. *J Colloid Interface Sci* 328:20–28. <https://doi.org/10.1016/j.jcis.2008.09.013>
- Beneš P, Paulenová M (1973) Surface charge and adsorption properties of polyethylene in aqueous solutions of inorganic electrolytes. *Colloid Polym Sci* 251:766–771. <https://doi.org/10.1007/BF01499104>
- Cadaval TR, Dotto GL, Seus ER, Mirlean N, Pinto LAA (2016) Vanadium removal from aqueous solutions by adsorption onto chitosan films. *Desalin Water Treat* 57:16583–16591. <https://doi.org/10.1080/19443994.2015.1079741>
- Calagui MJC, Senoro DB, Kan CC, Salvacion JW, Futralan CM, Wan MW (2014) Adsorption of indium(III) ions from aqueous solution using chitosan-coated bentonite beads. *J Hazard Mater* 277:120–126. <https://doi.org/10.1016/j.jhazmat.2014.04.043>
- Chen S, Yue Q, Gao B, Li Q, Xu X, Fu K (2012) Adsorption of hexavalent chromium from aqueous solution by modified corn stalk: a fixed-bed column study. *Bioresour Technol* 113:114–120. <https://doi.org/10.1016/j.biortech.2011.11.110>
- Dammak I, Sobral PJA (2018) Investigation into the physicochemical stability and rheological properties of rutin emulsions stabilized by chitosan and lecithin. *Food Eng* 229:12–20. <https://doi.org/10.1016/j.jfoodeng.2017.09.022>
- Deng Y, Wang L, Hu X, Liu B, Wei Z, Yang S, Sun C (2012) Highly efficient removal of tannic acid from aqueous solution by chitosan-coated attapulgite. *Chem Eng J* 181–182:300–306. <https://doi.org/10.1016/j.cej.2011.11.082>
- Donida MW, Rocha SCS (2002) Coating of urea with an aqueous polymeric suspension in a two-dimension spouted bed. *Dry Technol* 20: 685–704. <https://doi.org/10.1081/DRT-120002824>
- Dotto GL, Ocampo-Pérez R, Moura JM, Cadaval TRS Jr, Pinto LAA (2016) Adsorption rate of reactive black 5 on chitosan based materials: geometry and swelling effects. *Adsorption* 22:973–983. <https://doi.org/10.1007/s10450-016-9804-y>
- Futralan CM, Kan CC, Dalida ML, Pascua C, Wan MW (2011) Fixed-bed column studies on the removal of copper using chitosan immobilized on bentonite. *Carbohydr Polym* 83:697–704. <https://doi.org/10.1016/j.carbpol.2010.08.043>
- Gama MS, Luna FMT, Albarelli JQ, Beppu MM, Vieira RS (2018) Adsorption of copper on glass beads coated with chitosan: stirred batch and fixed bed analysis. *Can J Chem Eng* 95:1164–1170. <https://doi.org/10.1002/cjce.22813>
- German-Heins J, Flury M (2000) Sorption of Brilliant Blue FCF in soils as affected by pH and ionic strength. *Geoderma* 97:87–101. [https://doi.org/10.1016/S0016-7061\(00\)00027-6](https://doi.org/10.1016/S0016-7061(00)00027-6)
- Hashimoto T, Shiraki M, Sakai T (1975) Current reversal in the thermally stimulated current spectra of polyethylene. *Polymer Sci Part B* 13: 2401–2410. <https://doi.org/10.1002/pol.1975.180131214>
- Heinämäki JT, Lehtola VM, Nikupaavo P, Yliruusi JK (1994) The mechanical and moisture permeability properties of aqueous-based hydroxypropyl methylcellulose coating systems plasticized with polyethylene glycol. *Int J Pharm* 112:191–196. [https://doi.org/10.1016/0378-5173\(94\)90429-4](https://doi.org/10.1016/0378-5173(94)90429-4)
- Heise S, Wirth T, Höhlinger M, Hernández YT, Ortiz JAR, Wagener V, Virtanen S, Boccaccini AR (2018) Electrophoretic deposition of chitosan/bioactive glass/silica coatings on stainless steel and WE43 Mg alloy substrates. *Surf Coat Technol* 344:553–563. <https://doi.org/10.1016/j.surfcoat.2018.03.050>
- Jawad AH, Islam MA, Hameed BH (2017) Cross-linked chitosan thin film coated onto glass plate as an effective adsorbent for adsorption of reactive Orange 16. *Int J Biol Macromol* 95:743–749. <https://doi.org/10.1016/j.ijbiomac.2016.11.087>
- José MJS, Alvarez S, López R (2018) Catalytic combustion of vineyard pruning waste in a conical spouted bed combustor. *Catal Today* 305: 13–18. <https://doi.org/10.1016/j.cattod.2017.11.020>
- Larrosa APQ, Cadaval TRS Jr, Pinto LAA (2015) Influence of drying methods on the characteristics of a vegetable paste formulated by linear programming maximizing antioxidant activity. *LWT-Food Sci Technol* 60:178–185. <https://doi.org/10.1016/j.lwt.2014.08.003>
- Larrosa APQ, Camara AS, Pohndorf RS, Rocha SF, Pinto LAA (2018) Physicochemical, biochemical, and thermal properties of *Arthrospira (Spirulina)* biomass dried in spouted bed at different conditions. *Appl Phycol* 30:1019–1029. <https://doi.org/10.1007/s10811-017-1265-5>
- Li X, Anton N, Arpagaus C, Belleiteix F, Vandamme TF (2010) Nanoparticles by spray drying using innovative new technology: the Buchi Nano spray dryer B-90. *J Control Release* 147:304–310. <https://doi.org/10.1016/j.jconrel.2010.07.113>
- Marques JL Jr, Lütke SF, Frantz TS, Espinelli JBS Jr, Carapelli R, Pinto LAA, Cadaval TRS Jr (2018) Removal of Al (III) and Fe (III) from binary system and industrial effluent using chitosan films. *Int J Biol Macromol* 120:1667–1673. <https://doi.org/10.1016/j.ijbiomac.2018.09.135>
- Mohanarivivasan V, Mishra M, Paliwal JS, Singh SK, Selvarajan E, Suganthi V, Devi CS (2014) Studies on heavy metal removal efficiency and antibacterial activity of chitosan prepared from shrimp shell waste. *Biotech* 4:167–175. <https://doi.org/10.1007/s13205-013-0140-6>
- Marshall DW (2017) Spouted bed design considerations for coated nuclear fuel particles. *Powder Technol* 316:421–425. <https://doi.org/10.1016/j.powtec.2017.01.008>
- Mota J (2013) Solid solutions vs. solid dispersions: the impact of formulation. *Biomed Biopharm Res* 10:235–248
- Moura JM, Farias BS, Rodrigues DAS, Moura CM, Dotto GL, Pinto LAA (2015) Preparation of chitosan with different characteristics and its application for biofilms production. *Polym Environ* 23: 470–477. <https://doi.org/10.1007/s10924-015-0730-y>
- Moura CM, Moura JM, Soares NM, Pinto LA (2011) Evaluation of molar weight and deacetylation degree of chitosan during chitin deacetylation reaction: used to produce biofilm. *Chem Eng Prog* 50:351–355. <https://doi.org/10.1016/j.cep.2011.03.003>
- Nawi MA, Sabar S, Jawad AH, Sheilatina, Wan Ngah WS (2010) Adsorption of Reactive Red 4 by immobilized chitosan on glass plates: towards the design of immobilized TiO₂-chitosan synergistic photocatalyst-adsorption bilayer system. *Biochem Eng J* 49:317–325. <https://doi.org/10.1016/j.bej.2010.01.006>
- Niamnuy C, Kanthamool W, Devahastin S (2011) Hydrodynamic characteristics of a pulsed spouted bed of food particulates. *Food Eng* 103:299–307. <https://doi.org/10.1016/j.jfoodeng.2010.10.028>
- Nikšar A, Nasernejad B (2018) Modeling of gasification reaction to produce activated carbon from pistachio shells in a spouted bed. *Biomass Bioenergy* 119:97–108. <https://doi.org/10.1016/j.biombioe.2018.09.008>
- Pablos A, Aguado R, Tellabide M, Altzibar H, Freire FB, Bilbao J, Olazar M (2017) A new fountain confinement device for fluidizing fine and ultrafine sands in conical spouted beds. *Powder Technol* 328:38–46. <https://doi.org/10.1016/j.powtec.2017.12.090>
- Pâslaru E, Zemljic LF, Bračić M, Vesel A, Petričić I, Vasile C (2013) Stability of a chitosan layer deposited onto a polyethylene surface. *Appl Polym Sci* 130:2444–2457. <https://doi.org/10.1002/app.39329>
- Perazzini MTB, Freire FB, Ferreira MC, Freire JT (2017) Stability and performance of a spouted bed in drying skimmed milk: influence of the cone angle and air inlet device. *Dry Technol* 36:341–354. <https://doi.org/10.1080/07373937.2017.1331240>
- Piccin JS, Dotto GL, Pinto LAA (2011) Adsorption isotherms and thermochemical data of FD&C Red N° 40 binding by chitosan. *Braz J Chem Eng* 28:295–304. <https://doi.org/10.1590/S0104-66322011000200014>

- Piccin JS, Vieira MLG, Gonçalves JO, Dotto GL, Pinto LAA (2009) Adsorption of FD&C Red No. 40 by chitosan: isotherms analysis. *Food Eng* 95:16–20. <https://doi.org/10.1016/j.jfoodeng.2009.03.017>
- Popuri SR, Vijaya Y, Boddu VM, Abburi K (2009) Adsorptive removal of copper and nickel ions from water using chitosan coated PVC beads. *Bioresour Technol* 100:194–199. <https://doi.org/10.1016/j.biortech.2008.05.041>
- Prachayawarakorn S, Ruengnarong S, Soponronnarit S (2006) Characteristics of heat transfer in two-dimensional spouted bed. *Food Eng* 76:327–333. <https://doi.org/10.1016/j.jfoodeng.2005.05.028>
- Prakash N, Latha S, Sudha PN, Renganathan NG (2016) Kinetics of removal of chromium from wastewater using chitosan based binary polymer blends. *Synth React Inorg Met Org Chem* 46:1310–1317. <https://doi.org/10.1080/15533174.2015.1004456>
- Prakash N, Latha S, Sudha PN, Renganathan NG (2012a) Copper and cadmium removal from synthetic industrial wastewater using chitosan and nylon 6. *Environ Sci Pollut Res* 19:2930–2941. <https://doi.org/10.1007/s11356-012-0801-8>
- Prakash N, Sudha PN, Renganathan NG (2012b) Influence of clay on the adsorption of heavy metals like copper and cadmium on chitosan. *Environ Sci Pollut Res* 20:925–938. <https://doi.org/10.1007/s11356-012-0935-8>
- Rocha APT, Lisboa HM, Alsina OLS, Silva OS (2018) Coating process of *Phyllanthus niruri* Linn granules using spouted bed. *Powder Technol* 336:85–91. <https://doi.org/10.1016/j.powtec.2018.05.052>
- Rocha SCS, Donida MW, Marques AMM (2009) Liquid-particle surface properties on spouted bed coating and drying performance. *Can J Chem Eng* 87:695–703. <https://doi.org/10.1002/cjce.20208>
- Saygili H, Güzel F (2016) High surface area mesoporous activated carbon from tomato processing solid waste by zinc chloride activation: process optimization, characterization and dyes adsorption. *J Clean Prod* 113:995–1004. <https://doi.org/10.1016/j.jclepro.2015.12.055>
- Salih SS, Ghosh TK (2018) Adsorption of Zn (II) ions by chitosan coated diatomaceous earth. *Int J Biol Macromol* 106:602–610. <https://doi.org/10.1016/j.ijbiomac.2017.08.053>
- Schio RR, Rosa BC, Gonçalves JO, Pinto LAA, Mallmann ES, Dotto GL (2018) Synthesis of a bio-based polyurethane/chitosan composite foam using ricinoleic acid for the adsorption of Food Red 17 dye. *Int J Biol Macromol* 121:373–380. <https://doi.org/10.1016/j.ijbiomac.2018.09.186>
- Soares NM, Mendes TS, Vicente AA (2013) Effect of chitosan-based solutions applied as edible coatings and water glazing on frozen salmon preservation—a pilot-scale study. *Food Eng* 119:316–323. <https://doi.org/10.1016/j.jfoodeng.2013.05.018>
- Soares NM, Fernandes TA, Vicente AA (2016) Effect of variables on the thickness of an edible coating applied on frozen fish and establishment of the concept of safe dipping time. *Food Eng* 171:111–118. <https://doi.org/10.1016/j.jfoodeng.2015.10.016>
- Souza CRF, Donida MW, Rocha SCS, Oliveira WP (2009) The role of colloidal silicon dioxide on the enhancement of the drying of herbal preparations in suspended state. *Chem Eng Commun* 196:391–405. <https://doi.org/10.1080/00986440802359543>
- Tan IA, Ahmad AL, Hameed BH (2009) Fixed-bed adsorption performance of oil palm shell-based activated carbon for removal of 2,4,6-trichlorophenol. *Bioresour Technol* 100:1494–1496. <https://doi.org/10.1016/j.biortech.2008.08.017>
- Tripati S, Parthiban G, Pattan JN, Menezes A (2017) Chemical composition and provenance of Chinese porcelain shards recovered from Old Goa, west coast of India. *J Archaeol Sci Rep* 14:467–478. <https://doi.org/10.1016/j.jasrep.2017.06.002>
- Tutunaru B, Tigae C, Spînu C, Prunaru I (2017) Spectrophotometry and electrochemistry of Brilliant Blue FCF in aqueous solution of NaX. *Int J Electrochem Sci* 12:396–412. <https://doi.org/10.20964/2017.01.64>
- Vieira MLG, Martinez MS, Santos GB, Dotto GL, Pinto LAA (2018) Azo dyes adsorption in fixed bed column packed with different deacetylation degrees chitosan coated glass beads. *J Environ Chem Eng* 6:3233–3241. <https://doi.org/10.1016/j.jece.2018.04.059>
- Vieira MGA, Rocha SCS (2004) Influence of the liquid saturation degree on the fluid dynamics of a spouted-bed coater. *Chem Eng Process* 43:1275–1280. <https://doi.org/10.1016/j.ccep.2003.12.004>
- Vieira MLG, Esquerdo VM, Nobre LR, Dotto GL, Pinto LAA (2014) Glass beads coated with chitosan for the food azo dyes adsorption in a fixed bed column. *Ind Eng Chem* 20:3387–3393. <https://doi.org/10.1016/j.jiec.2013.12.024>
- Wan MW, Kan CC, Rogel BD, Dalida MLP (2010) Adsorption of copper (II) and lead (II) ions from aqueous solution on chitosan-coated sand. *Carbohydr Polym* 80:891–899. <https://doi.org/10.1016/j.carbpol.2009.12.048>
- Weska RF, Moura JM, Batista LM, Rizzi J, Pinto LAA (2007) Optimization of deacetylation in the production of chitosan from shrimp wastes: use of response surface methodology. *Food Eng* 80:749–753. <https://doi.org/10.1016/j.jfoodeng.2006.02.006>
- Withers R (2017) Elucidating the molecular behavior on the pH responsiveness of chitosan. *Chem Commun* 53:7373–7376. <https://doi.org/10.1039/C7CC01826F>
- Xua H, Matysiak S (2017) Effect of pH on chitosan hydrogel polymer network structure. *Chem Commun* 53:7373–7376. <https://doi.org/10.1039/c7cc01826f>
- Zargar V, Asghari M, Dashti A (2015) A review on chitin and chitosan polymers: structure, chemistry, solubility, derivatives, and applications. *Chem Bio Eng* 2:204–226. <https://doi.org/10.1002/cben.201400025>
- Zelkó R, Orban A, Süvegh K, Riedl Z (2002) Effect of plasticizer on the dynamic surface tension and the free volume of Eudragit systems. *Int J Pharm* 244:81–86. [https://doi.org/10.1016/S0378-5173\(02\)00317-4](https://doi.org/10.1016/S0378-5173(02)00317-4)

Publisher's note Springer Nature remains neutral with regard to jurisdictional claims in published maps and institutional affiliations.